PERGAMON

International Journal of Heat and Mass Transfer 42 (1999) 2849–2861

International Journal of HEAT and MASS TRANSFER

Computational study of laminar flow and mass transfer around a surface-mounted obstacle

G.B. Ngo Boum[a], S. Martemianov[b], A. Alemany[a,*]

[a] *Laboratoire des Ecoulements Géophysiques et Industriels, UMR CNRS NC5519, BP 53X-38041 Grenoble cedex, France*
[b] *Laboratoire d'Etudes Thermiques, UMR CNRS N6608, ESIP-40 avenue du Recteur Pineau 86022 Poitiers cedex, France*

Received 3 October 1997; in final form 20 October 1998

Abstract

Laminar mass transfer on a plane surface (electrode) deformed by a square micro-obstacle is numerically studied by simulating the flow and mass transfer at the solid/liquid interface. The obstacle has the same order of magnitude than the diffusion layer thickness and thus a linear approximation for the velocity profile is used at the inlet flow section. It is shown that the velocity profile in the normal direction, is disturbed in no more than three times the obstacle's height. It means that such micro-obstacle can be considered 'invisible' from the bulk flow point of view. On the other hand, the recirculating vortex behind the obstacle is found to have an enhancement effect on the mass transfer which is very important and strongly increases with the Reynolds and the Schmidt numbers.

Nomenclature

C active species local concentration
C_∞ active species bulk concentration
C_w active species wall concentration
C_τ wall shear coefficient
D active species diffusion coefficient
h obstacle height
H computational domain height
j wall current density
K mass transfer coefficient
k dimensional kinetic constant of the electrochemical reaction
k^* non-dimensional kinetic constant of the electrochemical reaction
L computational domain length
L_R recirculating region length
p pressure
p_0 reference pressure
S_0 wall velocity gradient at the inlet section
s non-dimensional curvilinear coordinate
u longitudinal velocity
u_0 reference velocity
v transversal velocity
x longitudinal coordinate
y transversal coordinate.

Greek symbols

δ diffusion boundary layer at the inlet flow section
μ dynamic viscosity
ν kinematic viscosity
ρ electrolyte density
τ wall shear stress
τ_0 wall shear stress at the inlet section.

Dimensionless numbers

Re_h $(= u_0 h/\nu)$ Reynolds number calculated with the obstacle height
Re_δ $(= u_0\delta/\nu)$ Reynolds number calculated with the diffusion layer thickness at the inlet section
Sc $(= \nu/D)$ Schmidt number
Sh $(= (\partial C/\partial y)|_{wall}/C_\infty/\delta)$ local value of the Sherwood number
Sh_0 value of the Sherwood number at the inlet section $(s = 0)$
Sh_m mean value of the Sherwood number.

* Corresponding author. Tel.: 0033 4 7682 5034; fax: 0033 4 7682 5271; e-mail: antoine.alemany@hmg.inpg.fr

0017–9310/99/$ - see front matter
PII: S0017–9310(98)00354–8

1. Introduction

The topic of this paper is to discuss the numerical computation of laminar flow and mass transfer around a surface mounted obstacle. During recent years, several papers dealing with flows past an enclosed or open backward-facing step [1, 2, 3], in a cavity [4, 5], and over a surface mounted obstacle [6, 7, 8], were published. These flows which abound in nature and in industrial applications can now be studied by means of numerical methods. Calculations of the above mentioned flow configurations are in reasonable agreement with experimental measurements and predict the main features of these flows, as for example flow separation and reattachment [7, 9]. The related problem of heat transfer in separation and reattachment regions has been studied as well [2, 9, 10] but not so intensively. The calculations of the effect on mass transfer remain rather limited [11, 12, 13].

There are two different situations when mass transfer around a surface mounted obstacle is studied. The first one deals with obstacles which are larger than the near-wall viscous layer. The flow perturbations from such large obstacles spread outside the viscous layer and can be a cause of some mechanical phenomena as for example increasing the hydrodynamical resistance. In order to treat the hydrodynamical problem in such a case, a specified velocity profile should be used as an upstream boundary condition.

The other situation is dealing with obstacles which are submerged into the viscous layer of the flow. It relates to a surface defect on a conducting wall or a protruding micro-electrode also embedded in a conducting wall. It is also connected with turbulence promoters located on a surface for the mass transfer enhancement. In order to treat the hydrodynamical problem in this case, a linear velocity profile can be used as an upstream boundary condition. Hydrodynamical perturbations from near-wall obstacles subside within the viscous layer and their effect on hydraulics characteristics, as for example on a resistance coefficient of the flow [14], are weak. Such obstacles can be called 'invisible' from a hydraulic point of view. Nevertheless, the above mentioned near-wall hydrodynamical disturbances can be sufficient to significantly perturbate the mass transfer. The situation is quite similar to turbulent mass transfer near a smooth surface where the near-wall velocity fluctuations do not influence the mean velocity profile but have an effect on the mass transfer.

From the numerical point of view, hydrodynamical and heat transfer problems are similar. Indeed, in the case of classical heat transfer problems, the Prandtl number is around $Pr \sim 1$–10, so the hydrodynamical and heat boundary layers are of the same order of magnitude and the numerical resolution is less complicated. For mass transfer problems the Schmidt number is very high (>1000) and the diffusion layer thickness is at least one order of magnitude smaller than the hydrodynamical one [15]. The same situation occurs for heat transfer in high viscosity and poorly heat conducting fluids when $Pr \sim 100$–1000. In the case of high Prandtl and Schmidt numbers, the numerical problem becomes sharper as a special care should be taken to the numerical grid.

Electrochemical processes are some of the important examples which are related to the present study. The fluid here, an electrolyte solution, is composed of electrochemical species and one of them, the electroactive species, reacts at the solid/liquid interface. Depending on the relative rate of the electrochemical process in comparison with that of the mass transport, different electrochemical regimes can be distinguished. The present study focuses on the situation where the electrode process is fast so the total reaction rate is controlled by mass transport. The electric current at the electrode is directly related to the mass flux. So, the resolution of mass transport problem provides the current distribution along the electrode. In this paper, hydrodynamics and mass transfer around surface mounted obstacle immersed into the viscous sublayer of an electrolyte flow is studied by means of numerical simulations.

2. Mathematical formulation

The situation examined here (Fig. 1) is that of an electrolyte flow along a plane electrode [AF]. The flow is disturbed by a square micro-obstacle [BCDE] of height h, located far enough from the leading edge of the electrode. Because the enhancement of mass transfer due to the perturbation is local, only a portion of the electrode [AF] surrounding the protruding obstacle is studied. Considering only the region in the very close vicinity of the wall, the velocity profile in the inlet section can be supposed linear. Therefore, the flow is characterised by the wall velocity gradient S_0. Concerning the mass transfer, it is characterised at the inlet section by means of mass flux density on the wall j_0 or diffusion layer thickness $\delta = DC_\infty/j_0$. A cubic approximation is used for the inlet concentration profile (to be precised later). The mass transfer is examined firstly for an infinite electrochemical reaction rate (diffusion limited regime) and secondly for a finite one.

2.1. Governing equations

Two-dimensional flow and mass transfer around a surface mounted obstacle can be described by means of the classical continuity, momentum and convection-diffusion equations [15].

To achieve the calculations, these equations and the corresponding boundary conditions are made dimensionless. The characteristic scales

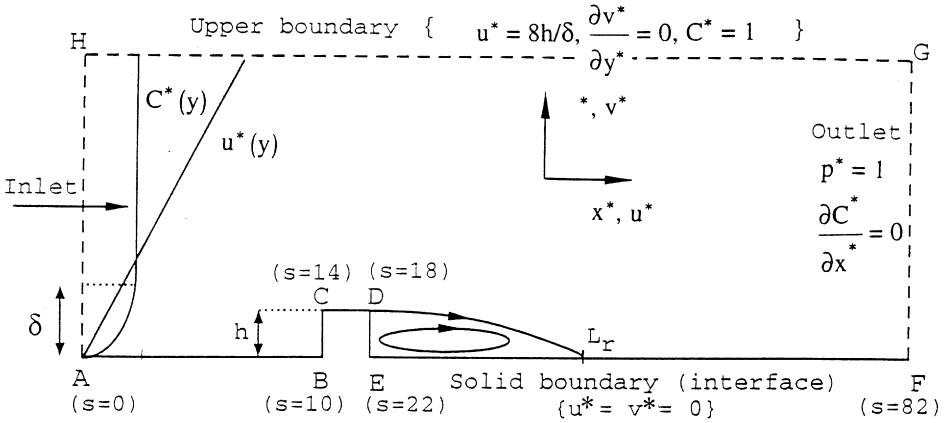

Fig. 1. Computational domain.

$\delta, u_0 = u(\delta)$ at the inlet section, $p_0 = \rho u_0^2, C_\infty$

the non-dimensional numbers

$$Sc = \frac{v}{D}, \quad Re_\delta = \frac{S_0 \delta^2}{v}$$

and the non-dimensional quantities

$$u^* = \frac{u}{u_0}, \quad v^* = \frac{v}{u_0}, \quad p^* = \frac{p}{p_0},$$

$$C^* = \frac{C}{C_\infty}, \quad x^* = \frac{x}{\delta}, \quad y^* = \frac{y}{\delta}$$

are used for that purpose. Therefore, the governing equations in non-dimensional form can be written as:

$$\frac{\partial u^*}{\partial x^*} + \frac{\partial v^*}{\partial y^*} = 0 \quad \text{(continuity)} \tag{1}$$

$$u^* \cdot \frac{\partial u^*}{\partial x^*} + v^* \cdot \frac{\partial u^*}{\partial y^*} = -\frac{\partial p^*}{\partial x^*} + \frac{1}{Re_\delta}\left(\frac{\partial^2 u^*}{\partial x^{*2}} + \frac{\partial^2 u^*}{\partial y^{*2}}\right)$$

(x-momentum) (2)

$$u^* \cdot \frac{\partial v^*}{\partial x^*} + v^* \cdot \frac{\partial v^*}{\partial y^*} = -\frac{\partial p^*}{\partial y^*} + \frac{1}{Re_\delta}\left(\frac{\partial^2 v^*}{\partial x^{*2}} + \frac{\partial^2 v^*}{\partial y^{*2}}\right)$$

(y-momentum) (3)

$$u^* \frac{\partial C^*}{\partial x^*} + v^* \frac{\partial C^*}{\partial y^*} = \frac{1}{Re_\delta \cdot Sc}\left(\frac{\partial^2 C^*}{\partial x^{*2}} + \frac{\partial^2 C^*}{\partial y^{*2}}\right) \quad \text{(mass)}$$

(4)

It should be noted here that another Reynolds number can also be introduced. This number is based on the height h and defined as $Re_h = S_0 h^2/v$ and is related by the factor $(\delta/h)^2$ to Re_δ.

The applied boundary conditions expressed in the dimensionless form are:

(i) wall boundary [ABCDEF]

- non slip condition at the wall
  $u^* = 0$ and $v^* = 0$
- finite or infinite electrochemical reaction rate

$$\left.\frac{\partial C^*}{\partial n}\right|_{\text{wall}} = k^* \cdot C_w^* \quad \text{or } C_w^* = 0 \quad (k^* = \to \infty)$$

where $k^* = \dfrac{k}{D/\delta}$ is the non-dimensional kinetic constant of the electrochemical reaction and n is the direction normal to the wall.

(ii) inlet boundary [AH]

- linear velocity profile
  $u^* = y^*$ and $v^* = 0$
- cubic profile approximation for concentration

$$\begin{cases} C^* = a_1 \cdot y^{*3} + a_2 \cdot y^{*2} + a_3 \cdot y^* + a_4 & \text{if } y^* < 1 \\ C^* = 1 & \text{if } y^* \geqslant 1 \end{cases}$$

The coefficients a_k are chosen so as to satisfy the following conditions:

- at the upper limit of the diffusion layer;

$$C^*(1) = 1 \quad \text{and} \quad \left.\frac{\partial C^*}{\partial y^*}\right|_{y^*=1} = 0 \tag{5}$$

- at the wall the condition (i) is supposed to be valid. Then the wall concentration and the mass flux can be written as

$$C_w^* = \frac{1}{1+k^*} \quad \text{and} \quad \left.\frac{\partial C^*}{\partial y^*}\right|_{y^*=0} = \frac{1}{1+1/k^*}. \tag{6}$$

This leads to the following expressions for the different coefficients,

$$a_1 = -\frac{k^*}{1+k^*}, \quad a_2 = \frac{k^*}{1+k^*},$$

$$a_3 = \left.\frac{\partial C^*}{\partial y^*}\right|_{y^*=0} = \frac{1}{1+1/k^*}, \quad a_4 = C_w^* = \frac{1}{1+k^*}. \tag{7}$$

When the electrode process is very fast, i.e. $k^* \gg 1$, those coefficients take the values:

$$a_1 = -1, \quad a_2 = 1, \quad a_3 = 1, \quad a_4 = C_w^* = 0. \tag{8}$$

(iii) upper boundary [HG]

- constant longitudinal velocity

$$u^* = 8h/\delta \quad \text{and} \quad \frac{\partial v^*}{\partial y^*} = 0$$

- bulk concentration

$$C^* = 1$$

(iv) outlet boundary [FG]

- constant pressure

$$p^* = 1$$

- zero longitudinal mass flux

$$\frac{\partial C^*}{\partial x^*} = 0$$

2.2. Numerical procedure

The equations were solved using the industrial code FLUENT which applies finite volume concepts to the discretisation of all the equations on a non-staggered grid. This code is not originally designed to deal with mass transfer problems, but rather with hydrodynamics and heat transfer, so special care was taken to the grid. In the following calculations the grid system is rectilinear with unequal spacing. Nodes are more closely spaced in the vicinity of the solid boundary and of the sharp edges of the surface mounted rib. Typically, the nodes spacing is ten times smaller around the rib and near the wall, so that the wall shear stress and the mass flux are more precisely calculated. The second order scheme QUICK is employed for the variable interpolation and the SIMPLEC algorithm is used for the resolution of the whole set of equations. The computations are performed on a Hewlett Packard HP700 computer, using a 105×45 non-uniform grid system. The grid elements distribution is chosen so that the diffusion layer is described with at least 10 elements for all cases. So the cells distribution is defined with respect to a less favorable case (corresponding here to a high value of the Reynolds number, $Re_h = 36.6$, and a high value of the Schmidt number $Sc = 2000$) and kept all along.

The numerical solution of momentum and continuity equations are first completed, then the obtained velocity and pressure fields are used to solve the electroactive species transport equation. To validate the numerical approach used in the present study, initial calculations are performed for the laminar mass transfer over a flat plate, known as the Levich problem [15]. The results are in good agreement with the existing analytical solution.

2.3. Computational domain

The computational domain height is chosen large enough so that the influence of the boundary conditions on the wall shear stress is very weak. Tests were made in order to determine that height and also the lengths upstream and downstream of the obstacle. It was found that the friction factor is varied within 10% of accuracy if the height H of the computational domain is varied from $H = 16h$ to $H = 5h$ and within 5% of accuracy if it is varied from $H = 16h$ to $H = 8h$. The height of the computational domain is then chosen such as; height [AH] $= H = 8h$. Furthermore, if the entrance length (before the obstacle) of the computational domain is about $10h$, the flow just after the inlet section boundary ($x = 0$) is not perturbated by the presence of the obstacle. Also, the length after the obstacle is chosen sufficiently large so that the perturbation generated by the obstacle is no more perceptible at the outlet section. So the total length is [ABEF] $= L = 71h$, except for the cases where only a qualitative estimation of the behaviour around the obstacle is necessary, in those cases [ABEF] $= L = 31h$.

3. Results and discussion

For the presentation of the results, we used the specific non-dimensional curvilinear coordinate s along the solid surface including the surface of the obstacle (using h as a reference scale). The different values of that coordinate are represented on Fig. 1. In order that the Figures be clear enough, the lengths along the obstacle have been stretched by a factor 4. Thus the values $10 \leqslant s \leqslant 14$ correspond to its front side [BC], $14 \leqslant s \leqslant 18$ to its upper side [CD] and $18 \leqslant s \leqslant 22$ to its rear side [DE].

3.1. Flow around surface mounted obstacle

Our goal is to study the influence of very small obstacles on the mass transfer rate. Figure 2 shows the rapid decay of the velocity perturbations within the viscous sublayer. In the normal (y) direction the velocity profile is not perturbated in a distance larger than 2–3 times the obstacle height. On the other hand, near the surface, velocity perturbations spread significantly downstream from the obstacle (Fig. 3).

Figures 4 and 5 show the local friction coefficient C_τ along the solid surface for different flow velocities (different values of Re_h). This quantity is defined as

$$C_\tau = \frac{\tau}{\mu \cdot u_0/\delta} \tag{9}$$

where

$$\tau = \mu \cdot \left.\frac{\partial u}{\partial y}\right|_{\text{wall}} \quad \text{or } \mu \cdot \left.\frac{\partial v}{\partial x}\right|_{\text{wall}} \tag{10}$$

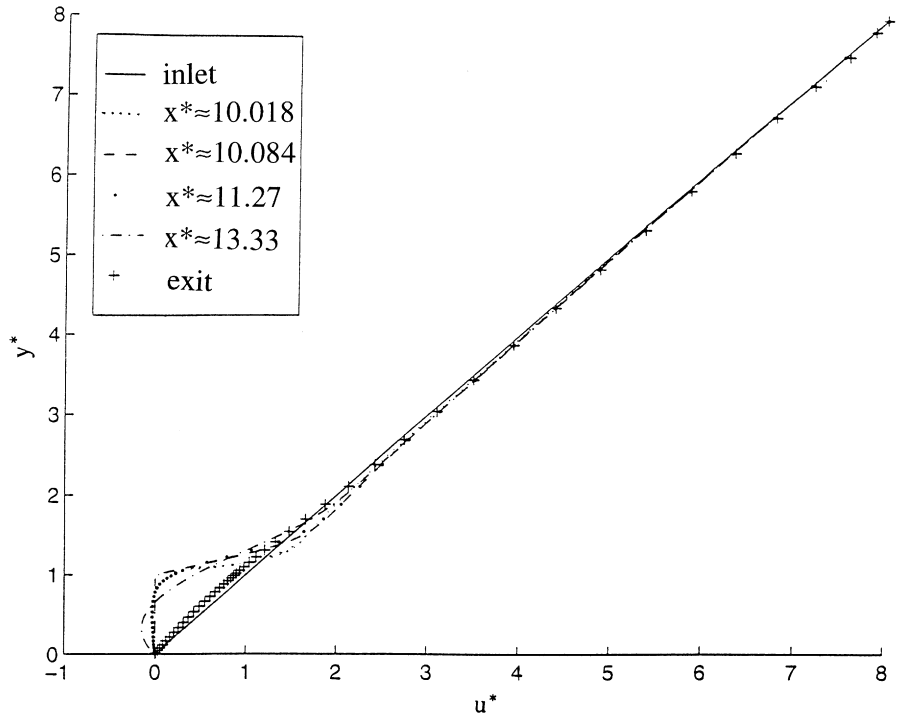

Fig. 2. Longitudinal velocity profiles at the inlet section ($x^* = 0$) and outlet section ($x^* = 31$), on the obstacle near the corners $x^* \sim 10.018$ and $x^* \sim 10.084$, and in the recirculating zone $x^* \sim 11.27$ and $x^* \sim 13.33$. $Re_h = 36.6$, $h = \delta$.

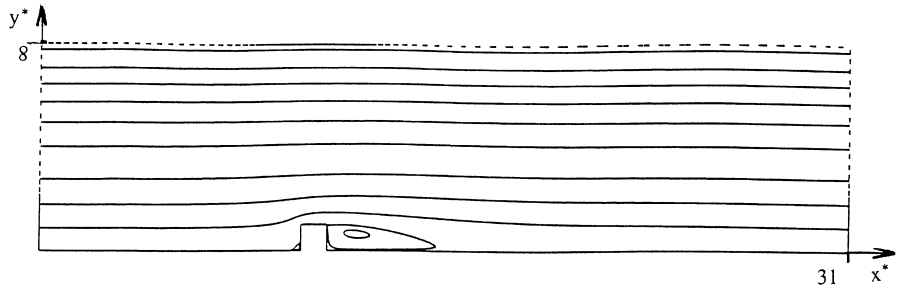

Fig. 3. Typical streamlines: $Re_h = 16.6$, $h = \delta$.

depending on the wall direction (horizontal or vertical respectively).

The influence of the obstacle on the flow upstream extend to a region which covers about 4–5 obstacle height. In that region the wall shear stress decreases monotonously down to the zero value. At the foot of the obstacle a small vortex is formed. There is no important influence of the Reynolds number Re_h on the velocity profile upstream from the obstacle.

On the front side of the obstacle, wall shear stress values are positive and increase monotonously if the Reynolds number is not too small ($Re_h \geqslant 3$). For small Reynolds numbers we can notice the existence of negative values of the wall shear stress. It means that a reattachment vortex is formed near the front side of the obstacle.

On the upper side of the obstacle a new boundary layer is formed. In this region the wall shear stress value is much more important than that at the inlet section ($x = 0$). The first peak which appears on Fig. 4, corresponds to the beginning of the upper viscous boundary layer. The local very thin thickness of this layer produces very high values of the shear stress. The influence of the Reynolds number on the wall shear stress is rather significant. The peak which appears at the end of the upper section of the obstacle can be explained by the sudden discontinuity at the corner of the obstacle. The same peaks were found as well in other numerical simu-

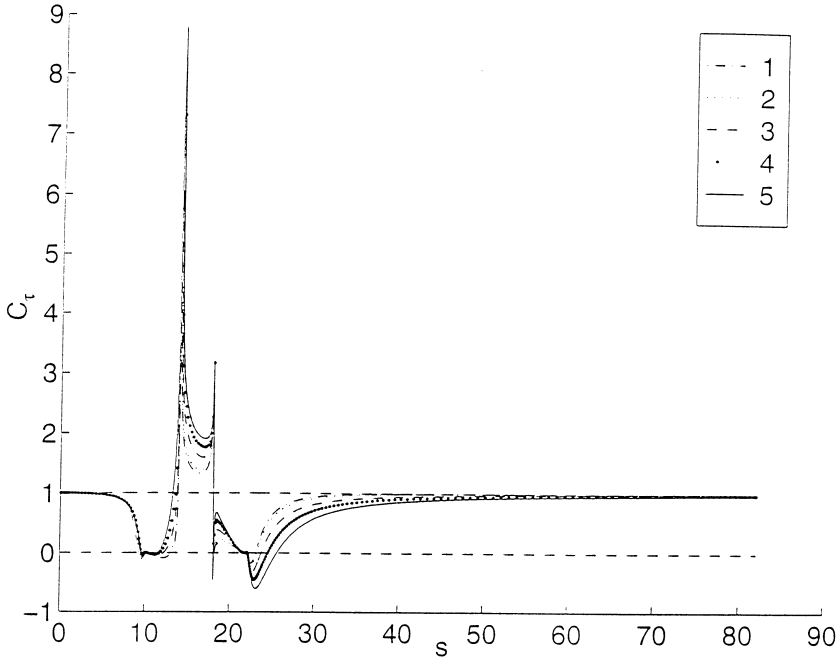

Fig. 4. Dimensionless wall shear stress coefficient for small values of Reynolds number: $Re_h = \{1: 0.66, 2: 1, 3: 3, 4: 5.98, 5: 10.6\}$, $h = \delta$.

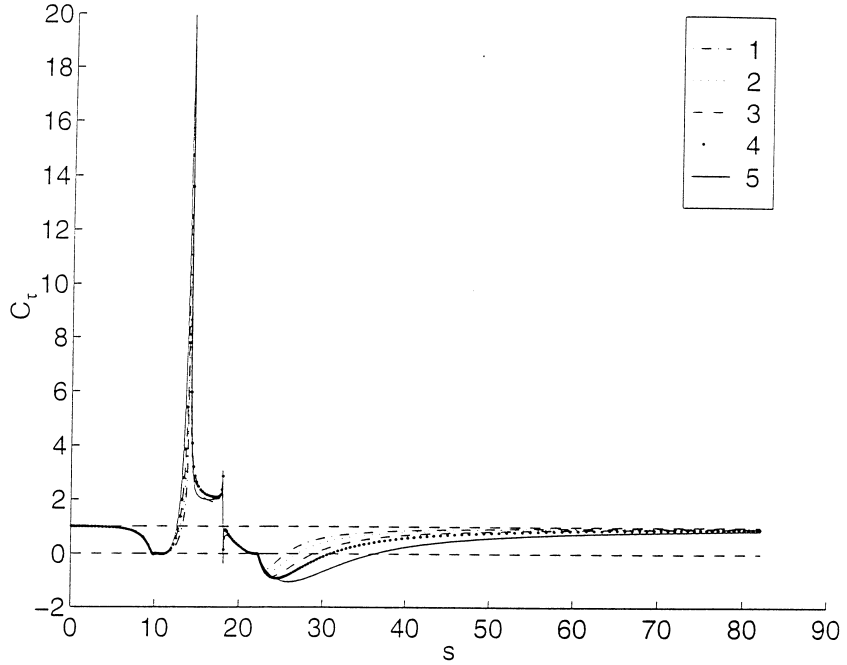

Fig. 5. Dimensionless wall shear stress coefficient for moderate values of the Reynolds number: {1: 10.6, 2: 16.6, 3: 26.6, 4: 36.6, 5: 66.4}, $h = \delta$.

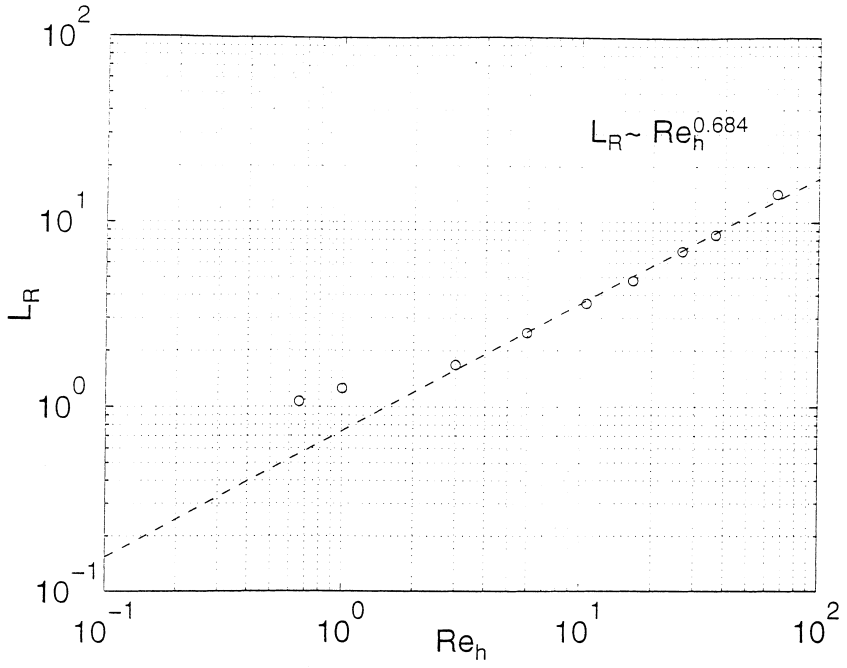

Fig. 6. Logarithmic plot of the recirculating flow length vs the Reynolds number: $h = \delta$, $Sc = 1000$.

lations of flow and heat or mass transfer around an obstacle [8, 10].

The rear side of the obstacle is characterised by small values of the wall shear stress. Downstream from the obstacle, a recirculating region corresponding to a vortex is formed. Its size can be characterised by the position of the reattachment point ($x = L_R$). It is obvious that the vortex size increases with the increasing Reynolds number (Fig. 6). After the flow reattachment, a new boundary layer is formed and the wall shear stress tends to its initial value. The flow behaviour moves back to the situation of a fluid flowing along a flat plate.

3.2. Mass transfer calculations

Figures 7 and 8 give the concentration profiles for different longitudinal positions and the isoconcentration lines. One can see the existence of a 'concentration eddy' downstream from the obstacle. The concentration profile in that zone has two 'diffusion layers'; one in the vicinity of the electrode surface and the other one at the upper limit between the recirculating zone and the external flow. The diffusion layer above the obstacle has no peculiarities, and its thickness is very small compared to the obstacle height.

The flow around the obstacle is characterised by one dimensionless parameter Re_δ. Two more parameters, the Schmidt number Sc and the ratio of the obstacle height to the diffusion layer thickness at the inlet, h/δ, have to be taken into account to characterise the mass transfer problem. The mass flux distribution along the surface for different values of the Reynolds number Re_δ is given on Figs 9 and 10 for $Sc = 1000$ and $h = \delta$. It is defined through the classical Sherwood number:

$$Sh = \frac{j \cdot \delta}{D \cdot C_\infty} \quad \text{where} \quad j = D \cdot \nabla C|_{\text{wall}} \tag{11}$$

with respect to the reference value at the inlet section.

3.2.1. Influence of the Reynolds number

Qualitatively, upstream and on the obstacle, the mass flux distribution is similar to the wall shear (Figs 9 and 10). So, we can observe that Reynolds analogy is quantitatively valid for this region. Everywhere on the upper side of the obstacle the mass transfer rate is more important than at the inlet.

Downstream from the obstacle, the influence of the recirculating vortex on mass transfer is noticeable. For the high value of Re_δ, that influence spreads very far. Mass flux and wall shear stress distributions downstream from the obstacle are qualitatively different. It means that Reynolds analogy cannot be used for the prediction of the mass transfer which is governed by a vortex. As shown on Fig. 7, the concentration gradient in the bulk of that region and thus the diffusion process is negligible. Convection carries fluid from the near-wall region where it is impoverished in active species by diffusion, to the upper

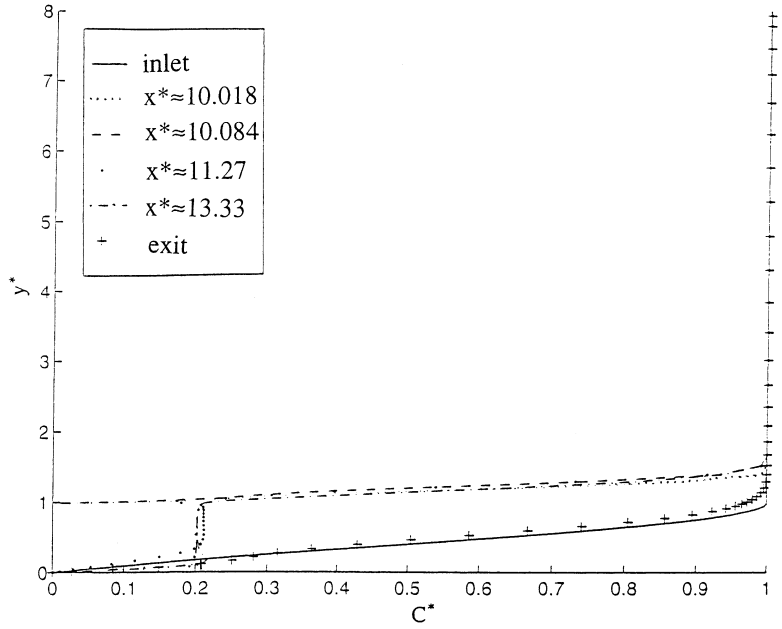

Fig. 7. Concentration profiles at different locations (obstacle = $x^* \sim 10.018$ and $x^* \sim 10.084$; recirculating zone = $x^* \sim 11.27$ and $x^* \sim 13.33$): $Re_h = 36.6$, $h = \delta$, $Sc = 1000$.

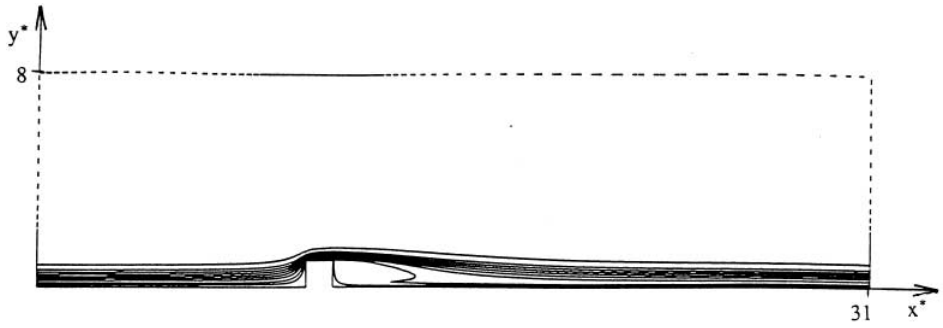

Fig. 8. Typical isoconcentration lines: $Re_\delta = 16.6$, $h = \delta$, $Sc = 1000$.

boundary of the recirculation zone where diffusion process tends again to enrich it in active species.

Plots of the mean value of the Sherwood number Sh_m defined as

$$Sh_m = \frac{1}{L_R}\int_{L_R} Sh(s)\,ds, \qquad L_R \text{ being the recirculating region length} \quad (12)$$

vs the Reynolds and Schmidt number on the recirculating region length (Fig. 11), characterises the evolution of the mass transfer. A correlation which supposes classical dependency with the Schmidt number (i.e. a Sherwood number varying as a power 1/3 of the Schmidt as it is the case for mass transfer on a flat plate) is searched on a power law form. The result obtained,

$$Sh_m = 0.0354 Re_h^{0.421} \cdot Sc^{0.333} \quad (13)$$

fits well with the numerical data. The exponent of the Reynolds number is not very far from the classical value, 0.5. The difference could be related to the fact that the eddy structure is the dominant parameter which depends on the Reynolds number. The situation is then not the same as in a classical problem characterised by a simple and imposed hydrodynamics corresponding to a boundary layer development along a flat plate. It can also be noticed on the Figure that for the low value of the Reynolds number, the Sherwood number is lower than one which is the value obtained without obstacle. This means that, in this condition, the recirculating motion in the vortex is not sufficiently intensive and then the transport of electroactive species by the vortex is less effective than

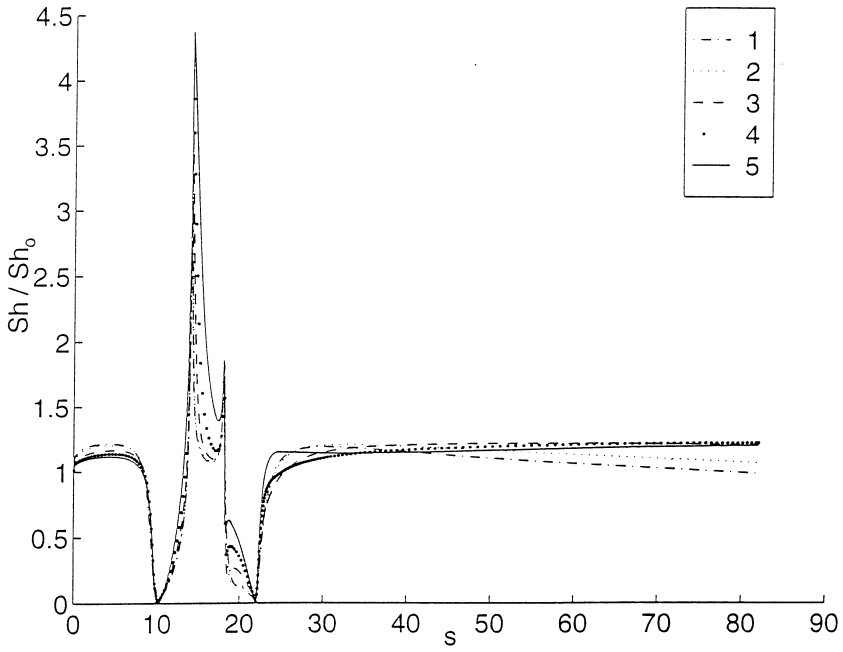

Fig. 9. Local Sherwood number for small values of the Reynolds number: $Re_h = \{1: 0.66, 2: 1, 3: 3, 4: 5.98, 5: 10.6\}$, $h = \delta$, $Sc = 1000$.

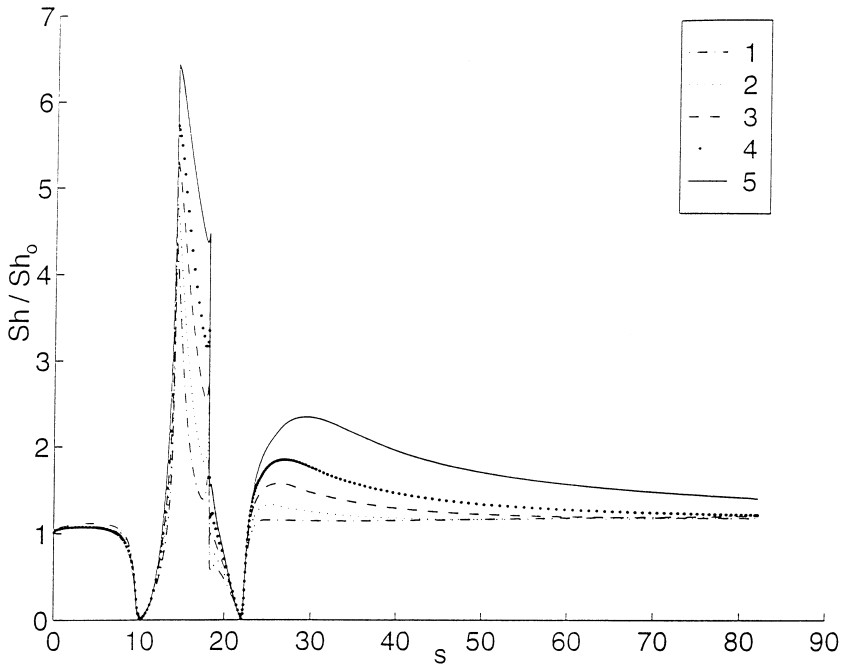

Fig. 10. Local Sherwood number for moderate values of the Reynolds number: $Re_h = \{1: 10.6, 2: 16.6, 3: 26.6, 4: 36.6, 5: 66.4\}$, $h = \delta$, $Sc = 1000$.

diffusivity of species across an unperturbated diffusive layer. When the Reynolds number increases the intensity of the downstream vortex also increases and for a typical value of the product $Re_h^{0.421} \cdot Sc^{0.333}$ larger than 30, the mass transfer is improved, compared to the reference value ~ 1.0.

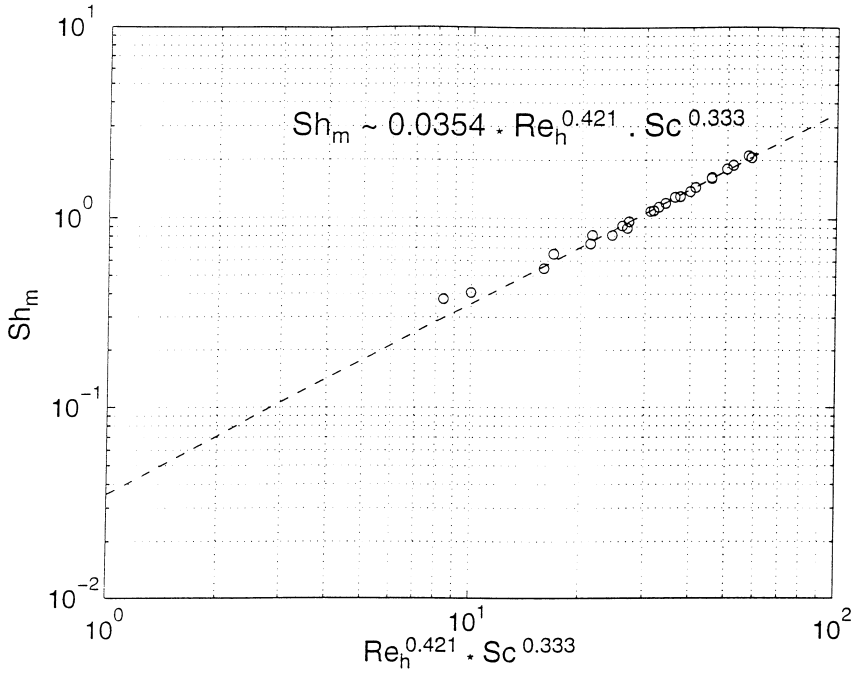

Fig. 11. Evolution of the mean value of the Sherwood number along the recirculating region length vs a correlation of the Reynolds and Schmidt numbers.

3.2.2. Influence of the Schmidt number

For given values of both velocity gradient and concentration profile at the inlet section, Figs 12 and 13 give the evolution of the mass transfer for different Schmidt numbers when an obstacle of size $h = \delta$ disturbs the flow. This evolution is characterised by the variation of the ratio $Sh/Sh_0(= Sh(s)/Sh(s = 0))$ along the curvilinear coordinate s, Sh_0 being the local value of the Sherwood number at the inlet ($s = 0$).

For a small value of the Reynolds number, Fig. 12 shows that the influence of the Schmidt number on the mass transfer is not very important. This results from the fact that the hydrodynamics perturbation is not intensive and limits by itself the exchange processes.

For moderately high values of the Reynolds number, Fig. 13 shows on the contrary that the mass transfer rate depends on the Schmidt number, especially in the regions where the hydrodynamics perturbation is high. This is the case, at the top of the obstacle (zone C–D, Fig. 1) and in the recirculating region behind the obstacle (zone of length L_R). For higher values of the Reynolds number (not shown here) that trend is confirmed.

3.2.3. Influence of the ratio h/δ

The influence of the ratio h/δ on the mass transfer rate is presented on Fig. 14 for constant Schmidt number: $Sc = 1000$ and Reynolds number: $Re_\delta = 16.6$. The mass transfer rate increases monotonously with the obstacle height, consequence of the increasing wall shear stress specifically in the recirculating flow region. Even for very small obstacles the mass transfer rate on the upper side of the obstacle is at least twice as much as that at the inlet section. If the height of the obstacle is two times the diffusion layer thickness, the mass transfer rate increases by about one order of magnitude in comparison with the inlet value. In this case, hydrodynamic perturbation of the mean flow can be expected.

3.2.4. Influence of the interfacial transfer rate

All the above mentioned results have concerned the case of infinite rate of the interfacial transfer process. If one takes into account the finite rate of the electrochemical reaction, one additional parameter appears (a non-dimensional kinetic constant k^*). Figure 15 demonstrates the influence of this parameter on the mass transfer rate. For slow reaction rates, k^* is about unity, the perturbation introduced by the obstacle does not influence the mass transfer. The local Sherwood number values Sh before and after the obstacle remains almost unchanged, in that case the charge transfer through the interface controls the electric current. For higher values of k^*, hydrodynamic influence appears. In agreement with the heterogeneous process theory [15], the maximum rate of the mass flux is obtained for a fully mass transport control regime, corresponding to infinite value of k^*.

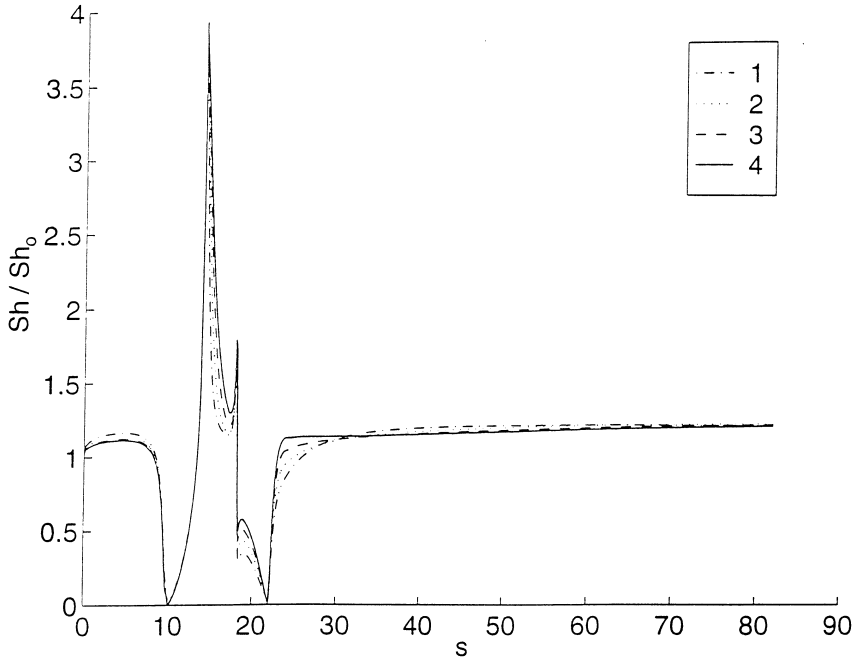

Fig. 12. Influence of the Schmidt number on the local Sherwood number for a small value of the Reynolds number: $Sc = \{1: 500, 2: 1000, 3: 1500, 4: 2000\}$, $Re_h = Re_\delta = 5.98$.

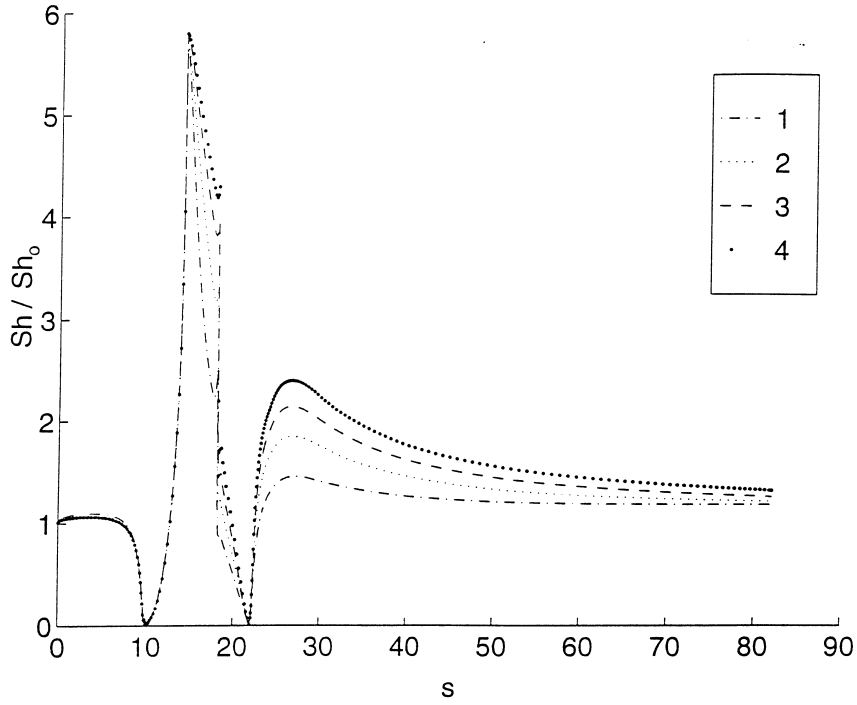

Fig. 13. Influence of the Schmidt number on the local Sherwood number for moderate values of the Reynolds number: $Sc = \{1: 500, 2: 1000, 3: 1500, 4: 2000\}$, $Re_h = Re_\delta = 36.6$.

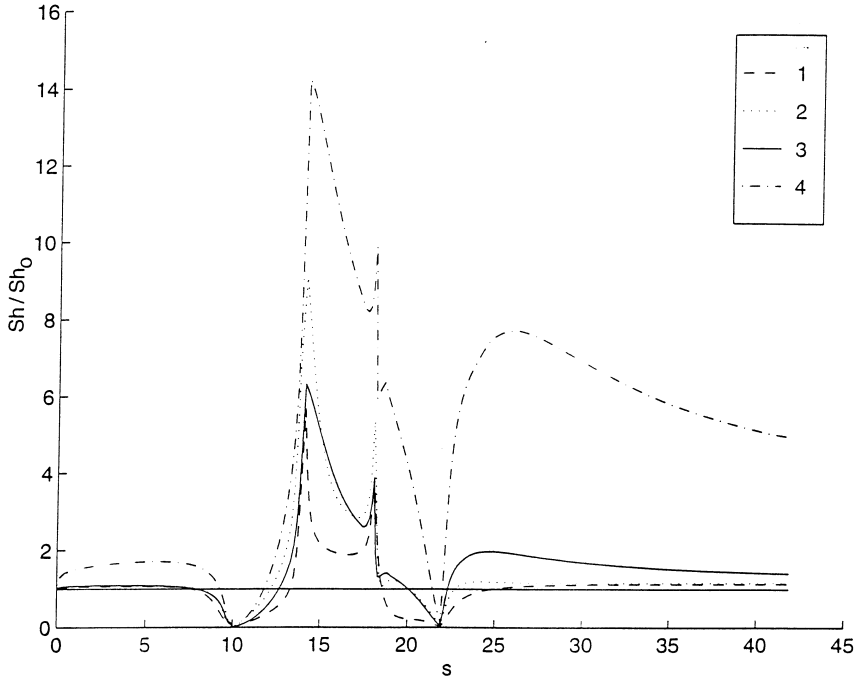

Fig. 14. Influence of the size of the obstacle on the local Sherwood number: {1: $h = 0.2\ \delta$, 2: $h = 0.6\delta$, 3: $h = \delta$, 4: $h = 2\delta$}, $Sc = 1000$.

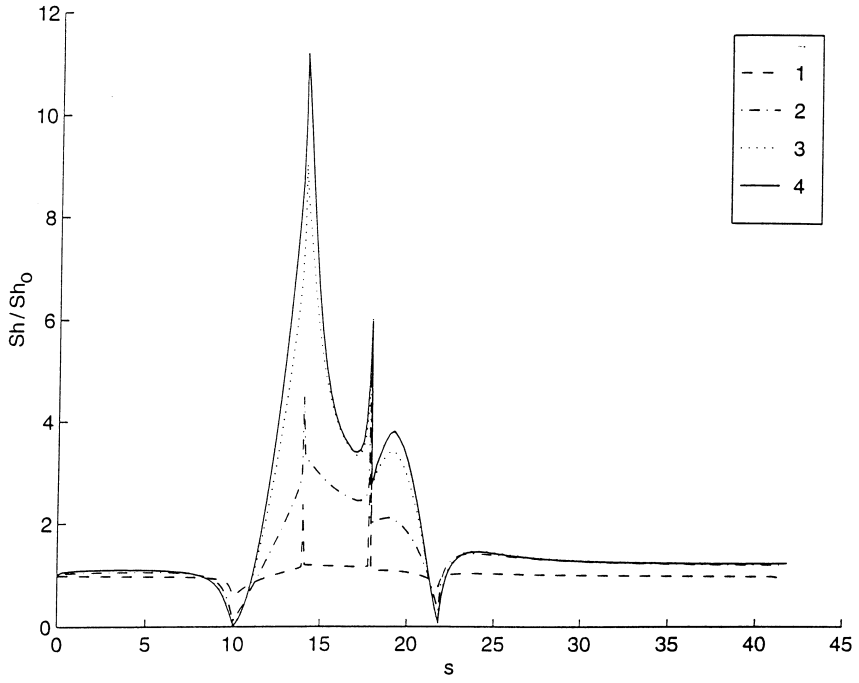

Fig. 15. Influence of the rate of the reaction on the local dimensionless Sherwood number, $h = \delta$: $Re_h = Re_\delta = 16.6$: {1: $k^* = 1$, 2: $k^* = 10$, 3: $k^* = 100$, 4: $k^* = \infty$}, $Sc = 1000$.

4. Conclusion

Numerical simulations of mass transfer in laminar flow show that micro-obstacles, hydrodynamically 'invisible' from the bulk flow point of view, may increase significantly the mass transfer rate. It means that for fast heterogeneous reactions the surface reactivity can be increased significantly by means of small modifications of the surface geometry. The increment in the mass transfer rate is due to two factors. At first, on the upper side of the obstacle it is induced by the local hydrodynamic boundary layer development. This factor has a local character, it means that the additional mass flux is proportional to the obstacle's surface. Another cause of that increment is the recirculating vortex. This vortex, formed downstream, is stretched in the flow direction and its influence covers an important zone. The mass transfer initiated by it, is quite different from the one in the developing diffusion layer. The concentration profile in this zone has two 'diffusion layers', in the vicinity of the surface and at the interface between the recirculating zone and the external flow. The consequence is that the Reynolds analogy cannot be used in order to predict the mass transfer which is governed by the near-wall eddy structures.

References

[1] I.E. Barton, Laminar flow past an enclosed and open backward-facing step, Physics of Fluids 6 (12) (1994) 4054–4056.

[2] M. Pingping, L. Xianming, N.K. David, Heat and mass transfer in a separated flow region for high Prandtl and Schmidt numbers under pulsatile conditions, Int. J. Heat and Mass Transfer 37 (17) (1994) 2723–2736.

[3] R.J. Goldstein, V.L. Ericksen, R.M. Olson, E.R.G. Eckert, Laminar separation, reattachment, and transition of the flow over a downstream-facing step, J. Basic Engineering, Trans. of ASME (1970) 732–741.

[4] A. Bhatti, W. Aung, Finite difference analysis of laminar separated forced convection in cavities, J. Heat Transfer 106 (2) (1984) 49–54.

[5] H. Nam Chang, H.W. Ryu, D.H. Park, et al., Effect of external laminar channel flow on mass transfer in a cavity, Int. J. Heat and Mass Transfer 30 (10) (1987) 2137–2149.

[6] S.S. Hsieh, D.Y. Huang, Flow characteristics of laminar separation on surface-mounted ribs, AIAA 25 (6) (1987) 819–823.

[7] Y.J. Hong, S.S. Hsieh, H.J. Shih, Numerical computation of laminar separation and reattachment of flow over surface-mounted ribs, J. Fluids Engineering, Trans. of ASME 133 (6) (1991) 190–198.

[8] F. Ferrigno, P.F. Brevet, H.H. Girault, Finite element simulation of the amperometric response of recessed and protruding microband electrodes in flow channels, J. Electroanalytical Chemistry 430 (1997) 235–242.

[9] T. Kondoh, Y. Nagano, T. Tsuji, Computational study of laminar heat transfer downward of a backward-facing step, Int. J. Heat and Mass Transfer 36 (3) (1993) 577–591.

[10] S.S. Hsieh, H.J. Shih, Y.J. Hong, Laminar forced convection from surface-mounted ribs, Int. J. Heat and Mass Transfer 33 (9) (1990) 1987–1999.

[11] P. Legentilhomme, J. Legrand, Modélisation numérique du transfert de matière dans un écoulement annulaire faiblement tourbillonnaire non entretenu, Can. J. Chem. Eng. 71 (1993) 299–311.

[12] M. Ould-Rouis, A. Salem, J. Legrand, C. Nouar, Etude numérique et expérimentale du transfert de matière et de quantité de mouvement dans un écoulement annulaire laminaire non établi, Int. J. Heat and Mass Transfer 38 (1995) 953–957.

[13] P. Olivas, F.H. Bark, On unsteady electrochemical coating of a cylinder at moderately large Reynolds number, Journal of Appl. Electrochemistry 27 (1997) 1369–1379.

[14] H. Schlichting, Boundary-layer Theory, 6th ed., McGraw-Hill Book Company, 1968.

[15] V.G. Levich, Physicochemical Hydrodynamics. Chap II, VI, Prentice-Hall, Inc., Englewood Cliffs, NJ, 1974.